



# Direct Observation of a Nonheme Iron(IV)–Oxo Complex That Mediates Aromatic C–F Hydroxylation

Sumit Sahu,<sup>†</sup> Matthew G. Quesne,<sup>‡</sup> Casey G. Davies,<sup>§</sup> Maximilian Dürr,<sup>||</sup> Ivana Ivanović-Burmazović,<sup>||</sup> Maxime A. Siegler,<sup>†</sup> Guy N. L. Jameson,<sup>\*,§</sup> Sam P. de Visser,<sup>\*,‡</sup> and David P. Goldberg<sup>\*,†</sup>

<sup>†</sup>Department of Chemistry, The Johns Hopkins University, 3400 North Charles Street, Baltimore, Maryland 21218, United States

<sup>‡</sup>Manchester Institute of Biotechnology and School of Chemical Engineering and Analytical Science, The University of Manchester, 131 Princess Street, Manchester M1 7DN, United Kingdom

<sup>§</sup>Department of Chemistry & MacDiarmid Institute for Advanced Materials and Nanotechnology, University of Otago, P.O. Box 56, Dunedin 9054, New Zealand

<sup>||</sup>Department of Chemistry and Pharmacy, University of Erlangen–Nürnberg, 91058 Erlangen, Germany

## S Supporting Information

**ABSTRACT:** The synthesis of a pentadentate ligand with strategically designed fluorinated arene groups in the second coordination sphere of a nonheme iron center is reported. The oxidatively resistant fluorine substituents allow for the trapping and characterization of an Fe<sup>IV</sup>(O) complex at –20 °C. Upon warming of the Fe<sup>IV</sup>(O) complex, an unprecedented arene C–F hydroxylation reaction occurs. Computational studies support the finding that substrate orientation is a critical factor in the observed reactivity. This work not only gives rare direct evidence for the participation of an Fe<sup>IV</sup>(O) species in arene hydroxylation but also provides the first example of a high-valent iron–oxo complex that mediates aromatic C–F hydroxylation.

Determining the first- and second-coordination sphere elements that control the reactivity of nonheme iron complexes has been the focus of intense efforts, in part because of the potential to identify the key factors that allow nonheme Fe enzymes to mediate an impressive array of oxidative transformations.<sup>1,2</sup> Learning how to rationally tune the reactivity of nonheme iron complexes also has direct implications for the development of earth-abundant, environmentally compatible catalysts. One subclass of nonheme Fe enzymes are pterin-dependent amino acid (AA) hydroxylases, which perform arene hydroxylations with mononuclear iron centers. A high-valent, electrophilic iron(IV)–oxo intermediate has been spectroscopically characterized as the active oxidant in two of these systems: Tyr and Phe hydroxylases.<sup>3</sup> Synthetic nonheme Fe complexes that promote arene hydroxylation have been known for over 20 years. Much speculation has centered on the nature of the active intermediate(s) in this chemistry, with proposals suggesting that Fe<sup>IV</sup>(O) or Fe<sup>V</sup>(O) intermediates may be the key players. However, direct evidence in these reactions for such high-valent intermediates is mostly unknown.<sup>1a,4</sup> Identification of the iron-based intermediate(s) that mediate arene hydroxylation remains a challenging goal.

Well-characterized Fe<sup>IV</sup>(O) species are strikingly inert in the oxidation of arene substrates.<sup>1a,4e,g,h</sup> However, the few

documented cases of *intramolecular* arene hydroxylation have been proposed to operate through putative Fe<sup>IV</sup>(O) intermediates.<sup>1a,4a–d</sup> We recently tested this dichotomy by constructing a nonheme iron(II) complex with two arene groups built into the second coordination sphere of [Fe<sup>II</sup>(N4Py<sup>2Ph</sup>)(CH<sub>3</sub>CN)]<sup>2+</sup>.<sup>1a</sup> Rapid *intramolecular* arene hydroxylation was observed, while, in contrast, no *intermolecular* arene hydroxylation chemistry could be seen for the Fe<sup>IV</sup>(O) complex of the untethered N4Py analog. Although indirect evidence suggested that an Fe<sup>IV</sup>(O) species was the active oxidant in the intramolecular case, we were unable to provide any direct observation of this elusive species.

Herein we have designed and synthesized a new ligand related to N4Py<sup>2Ph</sup>, in which fluorine groups were incorporated to allow for trapping of a putative Fe<sup>IV</sup>(O) intermediate. This ligand, N4Py<sup>2PhF<sub>2</sub></sup> (**1**), was used to prepare the new Fe<sup>II</sup> complex, [Fe<sup>II</sup>(N4Py<sup>2PhF<sub>2</sub></sup>)(NCMe)]<sup>2+</sup> (**2**), which then leads to trapping of an Fe<sup>IV</sup>(O) complex [Fe<sup>IV</sup>(O)(N4Py<sup>2PhF<sub>2</sub></sup>)]<sup>2+</sup> at low temperature as designed. However, upon controlled warming of the Fe<sup>IV</sup>(O) complex, an unprecedented arene C–F hydroxylation reaction occurs, resulting in formation of [Fe<sup>III</sup>(N4Py<sup>ArO,PhF<sub>2</sub></sup>)]<sup>2+</sup> (**3**). This controlled hydroxylation provided us with the first direct, time-dependent spectroscopic observations of a nonheme Fe<sup>IV</sup>(O) complex mediating arene hydroxylation. Density functional theory (DFT) studies support a mechanism involving electrophilic attack of Fe<sup>IV</sup>(O) on the arene substrate and indicate that proper orientation of the substrate is essential for reactivity. Although C–F cleavage of aromatic substrates has been observed for iron enzymes,<sup>5</sup> to our knowledge this report presents the first example of C–F hydroxylation mediated by a nonheme iron complex.

A polyfluorinated ligand, N4Py<sup>2PhF<sub>2</sub></sup> (**1**), was synthesized as shown in Scheme S1, and reaction of **1** with Fe<sup>II</sup>(BF<sub>4</sub>)<sub>2</sub> led to dark red crystals of [Fe<sup>II</sup>(N4Py<sup>2PhF<sub>2</sub></sup>)(CH<sub>3</sub>CN)](BF<sub>4</sub>)<sub>2</sub> (**2a**) (Figure 1) in 70% yield. The X-ray structure revealed a six-coordinate Fe<sup>II</sup> complex with CH<sub>3</sub>CN bound in the open site. The Fe–N distances are typical for low-spin (ls) iron(II) complexes,<sup>6</sup> which is consistent with Mössbauer spectroscopy (5.8 K,  $\delta$  = 0.49 mm s<sup>–1</sup>;  $\Delta E_Q$  = 0.54 mm s<sup>–1</sup>). The BF<sub>4</sub><sup>–</sup>

Received: July 19, 2014

Published: September 23, 2014

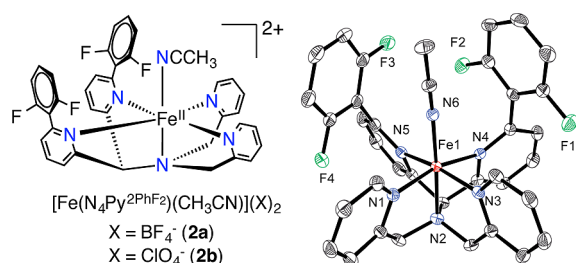


**Figure 1.**  $\text{Fe}^{\text{II}}$  complexes of **2a–b** (left), and displacement ellipsoid plot (50% probability) for the cation of **2a** (right). H-atoms were omitted for clarity.

counterion in **2a** can be replaced by  $\text{ClO}_4^-$ , giving  $\text{Fe}^{\text{II}}(\text{N}4\text{Py}^{2\text{PhF}_2})(\text{CH}_3\text{CN})(\text{ClO}_4)_2$  (**2b**) (X-ray structure, Figure S2). Both the  $\text{ClO}_4^-$  and  $\text{BF}_4^-$  complexes were employed in further reactivity studies (vide infra).

The iron(II) complexes **2a–b** react rapidly with a slight excess of the soluble O-atom transfer reagent isopropyl-2-iodoxybenzoate (IBX-ester) (1 equiv) in  $\text{CH}_3\text{CN}$  at 23 °C to immediately form a pale yellow intermediate with a weak absorption band at 750 nm. This yellow species then converts over 50 min into a dark green species with a more intense, red-shifted maximum at 785 nm (Figure 2). The weak band seen at

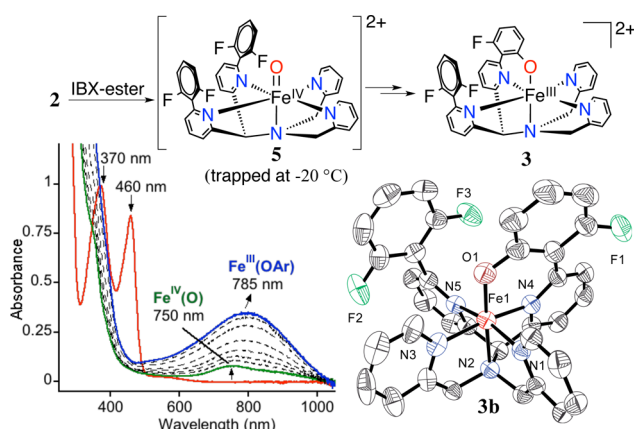


**Figure 2.** Overall scheme for aromatic hydroxylation (top), UV-vis spectral changes for **2a** + IBX-ester over 50 min in  $\text{CH}_3\text{CN}$  at 23 °C (bottom left), displacement ellipsoid plot (50% probability) for the dication of **3b** (bottom right). H-atoms were omitted for clarity.

750 nm is diagnostic of nonheme  $\text{Fe}^{\text{IV}}(\text{O})$  complexes.<sup>7</sup> However, the final spectrum with the more intense peak centered at 785 nm is suggestive of an  $\text{Fe}^{\text{III}}(\text{OAr})$  LMCT band.<sup>1a</sup> Analysis by LDI-MS of the final reaction mixture revealed a parent ion at  $m/z$  643.87 corresponding to  $[\text{Fe}(\text{N}4\text{Py}^{2\text{PhF}_2})+\text{O}-\text{F}]^+$  (calcd  $m/z$  644.14), suggesting that, remarkably, one of the C–F bonds had been cleaved and replaced by a C–O group. An isotope labeling experiment with  $\text{PhI}^{18}\text{O}$  shifts the peak at  $m/z$  643.8 by +2 units, confirming that the oxygen atom in the product comes from the oxidant (70% incorporation) (Figure S11). The monodefluorinated, monohydroxylated free ligand was isolated by demetalation and characterized by accurate mass determination by FAB-MS.

Definitive evidence for the occurrence of C–F hydroxylation was obtained by using the perchlorate starting material **2b**. Reaction of **2b** with 1 equiv of IBX-ester in  $\text{CH}_3\text{CN}$  led to the isolation of green crystals from  $\text{Et}_2\text{O}/\text{CH}_3\text{CN}$  suitable for X-ray structure determination, which revealed the structure for

$[\text{Fe}^{\text{III}}(\text{N}4\text{Py}^{\text{ArO,PhF}_2})](\text{ClO}_4)_2$  (**3b**) (Figure 2). The Fe–N (1.951(4)–2.040(4) Å) and Fe–O (1.787(3) Å) bond lengths in **3b** are consistent with a related  $\text{ls}$  ( $S = 1/2$ )  $\text{Fe}^{\text{III}}(\text{OAr})$  complex.<sup>1a</sup> A very small amount of yellow-green crystals precipitated together with **3b**, and X-ray diffraction revealed that these crystals are the iron(III)–fluoride complex  $[\text{Fe}^{\text{III}}(\text{N}4\text{Py}^{2\text{PhF}_2})(\text{F})](\text{ClO}_4)_2$  (**4b**) (Figure S4). Bond lengths for **4b** are consistent with a high-spin ( $\text{hs}$ ) ( $S = 5/2$ )  $\text{Fe}^{\text{III}}$  ion.

Further characterization of reaction mixtures by EPR spectroscopy revealed a rhombic,  $\text{ls-Fe}^{\text{III}}$  signal with  $g$  2.42, 2.13, 1.90, as well as peaks for  $\text{hs-Fe}^{\text{III}}$  at  $g$  6.35, 4.24 (Figure S12). The  $\text{ls-Fe}^{\text{III}}$  spectrum is a close match to that seen for  $[\text{Fe}^{\text{III}}(\text{N}4\text{Py}^{\text{PhO,Ph}})(\text{BF}_4)_2]^{1a}$  and can be assigned to the phenolato–iron(III) complex **3a**. The  $\text{hs-Fe}^{\text{III}}$  signals may arise at least in part from the minor side-product **4a**. A yield of 75–80% for **3b** was measured by UV-vis spectroscopy on final reaction mixtures following hydroxylation.

Low-temperature methods were employed to trap the metastable 750 nm species seen in Figure 2. Addition of IBX-ester to **2a** in  $\text{CH}_3\text{CN}$  at –20 °C leads to the isosbestic conversion seen in Figure S17, with a final, weak band appearing at 750 nm ( $\epsilon = 250 \text{ M}^{-1} \text{ cm}^{-1}$ ). This spectrum is stable for at least 4 h at –20 °C. Cold-spray ionization mass spectrometry (CSIMS) was performed on the reaction run at –20 °C and revealed a parent ion at  $m/z$  331.5679 which matches  $[\text{Fe}^{\text{IV}}(\text{O})(\text{N}4\text{Py}^{2\text{PhF}_2})]^{2+}$  (calcd  $m/z$  331.5667). The Mössbauer spectrum for the  $^{57}\text{Fe}$ -labeled  $\text{Fe}^{\text{II}}$  starting material is shown together with the spectrum for  $^{57}\text{Fe}^{\text{IV}}(\text{O})(\text{N}4\text{Py}^{2\text{PhF}_2})^{2+}$  in Figure 3. The sharp doublet seen for the  $\text{Fe}^{\text{II}}$  complex clearly

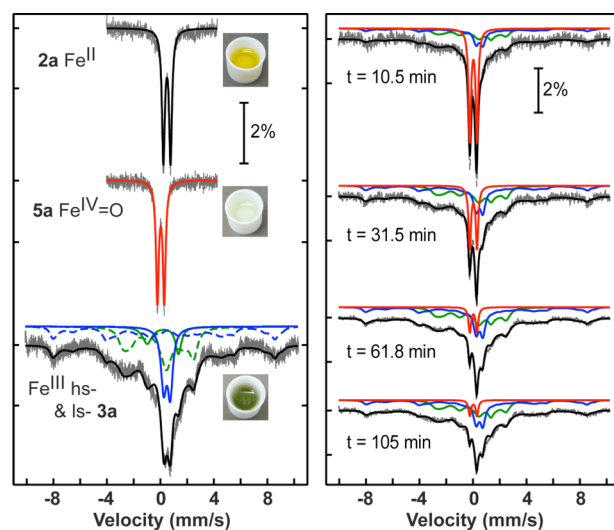


**Figure 3.** Mössbauer spectra (data collected at 5.8 K) for **2a**, **5a** and the final solution after warming **5a** (left) and time-dependent conversion of **5a** to **3a** (right).

shifts to a lower isomer shift upon oxidation, giving a new, sharp doublet characterized by  $\delta = 0.03 \text{ mm/s}$ ,  $\Delta E_Q = 0.54 \text{ mm/s}$ . The low isomer shift is a hallmark of an  $\text{Fe}^{\text{IV}}(\text{O})$  complex (**5a**). The quadrupole splitting parameter for this species is smaller than the  $\Delta E_Q$  values observed for most other  $\text{ls-Fe}^{\text{IV}}(\text{O})$  complexes<sup>7</sup> and falls closer to those for high-spin ( $S = 2$ )  $\text{Fe}^{\text{IV}}(\text{O})$  complexes. However, density functional theory (DFT) calculations suggest that **5a** has a low-spin ( $S = 1$ ) ground state (vide infra).

Gradual warming of the  $\text{Fe}^{\text{IV}}(\text{O})$  complex **5a** from –20 to 23 °C triggers the direct conversion of the weak band at 750 nm

(yellow) to the relatively intense band at 780 nm (green) for  $[\text{Fe}^{\text{III}}(\text{N4Py}^{\text{ArO,PhF}_2})]^{2+}$ . These spectral changes are similar to those seen at room temperature. This conversion was also monitored by CSIMS. The mass spectrum for **5a** disappears upon warming, and a new spectrum is observed with a parent ion at  $m/z$  322.0679, which matches the expected peak for **3a** ( $[\text{Fe}^{\text{III}}(\text{N4Py}^{\text{ArO,PhF}_2})]^{2+}$  (calcd:  $m/z$  322.0675). The EPR spectrum for **5a** generated at  $-20^\circ\text{C}$  is featureless as expected, except for a residual high-spin  $\text{Fe}^{\text{III}}$  spectrum ( $g = 4.22$ ). Upon warming, the EPR spectrum revealed peaks at  $g$  2.42, 2.13, 1.90, indicative of the  $\text{ls-Fe}^{\text{III}}(\text{OAr})$  complex **3a**. The kinetics of conversion to the C–F hydroxylation product could also be directly monitored by UV–vis spectroscopy at rt, where the 750 nm band was shown to convert directly into the 785 nm species. A plot of absorbance at 785 nm versus time fit well to a first-order kinetic model up to 5 half-lives (Figure S24). Fitting of the data yielded a first-order rate constant of  $k = 0.9 \times 10^{-3} \text{ s}^{-1}$ . The rate constant is independent of the concentration of the iron complex, supporting an intramolecular mechanism for the C–F hydroxylation.

Time-dependent Mössbauer spectroscopy provided conclusive evidence for the intermediacy of the  $\text{Fe}^{\text{IV}}(\text{O})$  species in C–F hydroxylation (Figure 3). The  $\text{Fe}^{\text{IV}}(\text{O})$  complex **5a** was first generated at  $-20^\circ\text{C}$  and then was slowly warmed and allowed to react at  $15\text{--}19^\circ\text{C}$  for varying reaction times. The doublet for **5a** smoothly converts to a new spectrum over 105 min. This new spectrum consists of a mixture of *hs* (blue) and *ls* (green)  $\text{Fe}^{\text{III}}$  signals that are both slow (dashed lines) and fast (solid lines) relaxing. The isomer shift and quadrupole splittings of both  $\text{Fe}^{\text{III}}$  species were determined by measuring the sample at 170 K, at which temperature the spectrum almost fully relaxes into a set of quadrupole doublets (*hs-Fe*<sup>III</sup>:  $\delta$  0.49 mm/s,  $\Delta E_Q = 0.49$  mm/s; *ls-Fe*<sup>III</sup>:  $\delta$  0.18 mm/s,  $\Delta E_Q = 2.33$  mm/s). The full hyperfine constants are given in Tables S1–S2. The relative area of each species was determined at different time points, and the data are plotted in Figure S23. The  $\text{Fe}^{\text{IV}}(\text{O})$  complex undergoes a single exponential decay with a rate constant of  $k = 1.2 \times 10^{-3} \text{ s}^{-1}$ , which is in excellent agreement with the rate constant determined by UV–vis spectroscopy. Upon warming the  $\text{Fe}^{\text{IV}}(\text{O})$  complex trapped at  $-20^\circ\text{C}$ , equal proportions of *hs*- and *ls-Fe*<sup>III</sup> species are produced. Although the *ls-Fe*<sup>III</sup> species can be assigned to **3a**, the *hs-Fe*<sup>III</sup> component may partly be composed of the  $\text{Fe}^{\text{III}}(\text{F})$  side-product **4a** as noted earlier. However, a hydroxylation reaction carried out at rt and then subsequently frozen for Mössbauer spectroscopy showed higher proportions of *ls-Fe*<sup>III</sup>, more consistent with the higher yields of **3a** obtained by UV–vis.

Taken together, all of the data indicate that the  $\text{Fe}^{\text{IV}}(\text{O})$  species is the key intermediate that initiates the arene hydroxylation reaction. Electrophilic attack of  $\text{Fe}^{\text{IV}}(\text{O})$  on the deactivated, difluorophenyl ring in  $[\text{Fe}^{\text{IV}}(\text{O})(\text{N4Py}^{2\text{PhF}_2})]^{2+}$  is the most reasonable next step, with electron transfer from the arene ring to the Fe center to give an arene radical concomitant with C–O bond formation. The release of a fluorine radical is unfavorable, and therefore it is more likely that the radical intermediate is reduced by one electron from an as yet unidentified reductant, allowing for the facile elimination of  $\text{F}^-$  and formation of **3**. A recent example of a C–F hydroxylation reaction mediated by a high-valent copper species is also promoted by a sacrificial reductant.<sup>8</sup>

DFT calculations were performed to analyze the initial electrophilic attack of the  $\text{Fe}^{\text{IV}}(\text{O})$  species (Figure 4). The calculations indicate a triplet spin ground state for **5**, with a low-

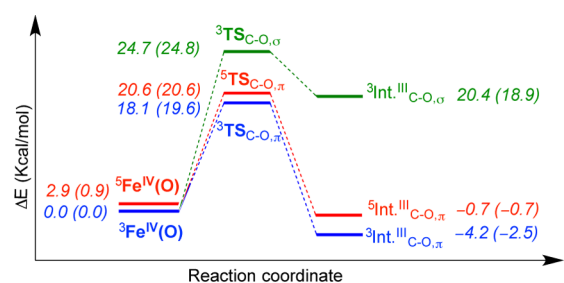


**Figure 4.** Potential energy diagram for the initial electrophilic attack of **5**. The numbers in parentheses are  $\Delta G$  at 298 K.

lying quintet excited state. The O-atom attacks the aromatic ring via transition states  ${}^{3,5}\text{TS}_{\text{C-O}}$ , leading to stable radical intermediates  ${}^{3,5}\text{Int}^{\text{III}}_{\text{C-O}}$ . The triplet spin pathway is the lowest in energy, proceeding via  ${}^3\text{TS}_{\text{C-O},\pi}$  (18.1 kcal/mol), which is unusual in nonheme iron reactivity because the high-spin quintet barrier is normally lower in energy.<sup>4g,9</sup> The triplet spin state is calculated to react by accepting an electron into a  $\pi^*_{xz/yz}$  orbital ( $\pi$ -pathway), which requires the substrate to orient with an angle of  $\text{Fe-O-C} \approx 120^\circ$  for good overlap. In contrast, the quintet spin state can, in principle, react through an additional channel involving one electron transfer to a  $\sigma^*_{z^2}$  orbital ( $\sigma$ -pathway,  $\text{Fe-O-C} \approx 180^\circ$ ), because this acceptor orbital comes down in energy for the quintet state. An orientation with  $\text{Fe-O-C} = 116.8^\circ$  ( $116.0^\circ$ ) is obtained for  ${}^3\text{TS}_{\text{C-O}}$  ( ${}^5\text{TS}_{\text{C-O}}$ ) indicating that the aromatic attack takes place via a  $\pi$ -pathway for both spin states. Group spin densities also confirm  $\pi$ -pathways for both states. Attempts to swap orbitals and create  $\sigma$ -pathway intermediates and TSs in the quintet spin state failed, converging back to the lower lying solutions described in Figure 4. Typically, the triplet  $\pi$ -pathway, which requires an approximate perpendicular substrate approach, is prohibitively high in energy because of the steric clash with the equatorial ligands, preventing *intermolecular* arene hydroxylation.<sup>4g,10</sup> Thus, orientation of the substrate in the second coordination sphere of  $[\text{Fe}^{\text{IV}}(\text{O})(\text{N4Py}^{2\text{PhF}_2})]^{2+}$  has caused a dramatic lowering of the triplet  $\pi$ -pathway. The availability of this pathway is likely responsible for the observed intramolecular arene hydroxylation, as proposed previously.<sup>1a</sup>

Conclusive evidence has been provided to show that aromatic C–F hydroxylation is mediated by a metastable  $\text{Fe}^{\text{IV}}(\text{O})$  intermediate. A key aspect of the inherent reactivity of the  $\text{Fe}^{\text{IV}}(\text{O})$  complex comes from the proper orientation of the arene substrate in the second coordination sphere. In an earlier study, we showed that positioning of a phenyl ring in the second-coordination sphere of  $[\text{Fe}^{\text{II}}(\text{N4Py}^{2\text{Ph}})]^{2+}$  facilitated arene hydroxylation and postulated that this reaction proceeded via a key, yet unidentified  $\text{Fe}^{\text{IV}}(\text{O})$  intermediate. In the current work we successfully arrested the arene hydroxylation chemistry through fluorination of the second-coordination sphere Ph groups, allowing for the  $\text{Fe}^{\text{IV}}(\text{O})$  intermediate to be trapped and characterized. However, this intermediate was still capable of intramolecular arene hydroxylation at higher temperatures and its direct conversion into hydroxylated product could be monitored in real time. These results together with DFT calculations help to clarify long-standing, yet puzzling observations in the literature<sup>1a,4c,e,g,h</sup> that indicate that  $\text{Fe}^{\text{IV}}(\text{O})$  species can mediate *intramolecular*, but not *intermolecular*, arene hydroxylations. These studies suggest that the inherent reactivity of *ls-Fe*<sup>IV</sup>(O) complexes could be unleashed through further ligand design to facilitate challenging reactions. These results also



support the importance of substrate orientation in tuning the reactivity at the metal center of nonheme Fe enzymes.

## ■ ASSOCIATED CONTENT

### ■ Supporting Information

Experimental and DFT details, Scheme S1, Tables S1–S10, and Figures S1–S28. This material is available free of charge via the Internet at <http://pubs.acs.org>.

## ■ AUTHOR INFORMATION

### Corresponding Authors

dpg@jhu.edu

gjamson@chemistry.otago.ac.nz

sam.devisser@manchester.ac.uk

### Notes

The authors declare no competing financial interest.

## ■ ACKNOWLEDGMENTS

The NIH (D.P.G., GM62309) is acknowledged for financial support. S.S. is grateful for a Martin and Mary Kilpatrick Fellowship. S.d.V. thanks the NSCCS for CPU time, and M.G.Q. thanks the BBSRC for a studentship. G.N.L.J. thanks The International Mobility Fund administered by Royal Society of New Zealand. I.I.-B. and M.D. acknowledge the “Solar Technologies Go Hybrid” initiative of the State of Bavaria.

## ■ REFERENCES

- (1) (a) Sahu, S.; Widger, L. R.; Quesne, M. G.; de Visser, S. P.; Matsumura, H.; Moëne-Loccoz, P.; Siegler, M. A.; Goldberg, D. P. *J. Am. Chem. Soc.* **2013**, *135*, 10590–10593. (b) Widger, L. R.; Davies, C. G.; Yang, T.; Siegler, M. A.; Troeppner, O.; Jameson, G. N. L.; Ivanović-Burmazović, I.; Goldberg, D. P. *J. Am. Chem. Soc.* **2014**, *136*, 2699–2702.
- (2) (a) Krebs, C.; Fujimori, D. G.; Walsh, C. T.; Bollinger, J. M., Jr. *Acc. Chem. Res.* **2007**, *40*, 484–492. (b) Bruijninx, P. C. A.; van Koten, G.; Klein Gebbink, R. J. M. *Chem. Soc. Rev.* **2008**, *37*, 2716–2744.
- (3) (a) Eser, B. E.; Barr, E. W.; Frantom, P. A.; Saleh, L.; Bollinger, J. M., Jr.; Krebs, C.; Fitzpatrick, P. F. *J. Am. Chem. Soc.* **2007**, *129*, 11334–11335. (b) Panay, A. J.; Lee, M.; Krebs, C.; Bollinger, J. M., Jr.; Fitzpatrick, P. F. *Biochemistry* **2011**, *50*, 1928–1933.
- (4) (a) Hegg, E. L.; Ho, R. Y. N.; Que, L., Jr. *J. Am. Chem. Soc.* **1999**, *121*, 1972–1973. (b) Mekmouche, Y.; Ménage, S.; Toia-Duboc, C.; Fontecave, M.; Galey, J.-B.; Lebrun, C.; Pécaut, J. *Angew. Chem., Int. Ed.* **2001**, *40*, 949–952. (c) Jensen, M. P.; Lange, S. J.; Mehn, M. P.; Que, E. L.; Que, L., Jr. *J. Am. Chem. Soc.* **2003**, *125*, 2113–2128. (d) Mehn, M. P.; Fujisawa, K.; Hegg, E. L.; Que, L., Jr. *J. Am. Chem. Soc.* **2003**, *125*, 7828–7842. (e) Oh, N. Y.; Seo, M. S.; Lim, M. H.; Consugar, M. B.; Park, M. J.; Rohde, J.-U.; Han, J.; Kim, K. M.; Kim, J.; Que, L., Jr.; Nam, W. *Chem. Commun.* **2005**, 5644–5646. (f) Nielsen, A.; Larsen, F. B.; Bond, A. D.; McKenzie, C. J. *Angew. Chem., Int. Ed.* **2006**, *45*, 1602–1606. (g) de Visser, S. P.; Oh, K.; Han, A.-R.; Nam, W. *Inorg. Chem.* **2007**, *46*, 4632–4641. (h) Makhlynets, O. V.; Rybak-Akimova, E. V. *Chem.—Eur. J.* **2010**, *16*, 13995–14006. (i) Thibon, A.; Jollet, V.; Ribal, C.; Sénéchal-David, K.; Billon, L.; Sorokin, A. B.; Banse, F. *Chem.—Eur. J.* **2012**, *18*, 2715–2724. (j) Bigi, J. P.; Harman, W. H.; Lassalle-Kaiser, B.; Robles, D. M.; Stich, T. A.; Yano, J.; Britt, R. D.; Chang, C. J. *J. Am. Chem. Soc.* **2012**, *134*, 1536–1542. (k) Ansari, A.; Kaushik, A.; Rajaraman, G. *J. Am. Chem. Soc.* **2013**, *135*, 4235–4249.
- (5) (a) Murphy, C. D. *Biotechnol. Lett.* **2010**, *32*, 351–359. (b) Fox, B. G.; Borneman, J. G.; Wackett, L. P.; Lipscomb, J. D. *Biochemistry* **1990**, *29*, 5300–5306.
- (6) Prat, I.; Company, A.; Corona, T.; Parella, T.; Ribas, X.; Costas, M. *Inorg. Chem.* **2013**, *52*, 9229–9244.
- (7) McDonald, A. R.; Que, L., Jr. *Coord. Chem. Rev.* **2013**, *257*, 414–428.
- (8) Serrano-Plana, J.; Garcia-Bosch, I.; Miyake, R.; Costas, M.; Company, A. *Angew. Chem. Int. Ed.* **2014**, *53*, 9608–9612.

- (9) (a) de Visser, S. P. *J. Am. Chem. Soc.* **2006**, *128*, 9813–9824. (b) Hirao, H.; Kumar, D.; Que, L., Jr.; Shaik, S. *J. Am. Chem. Soc.* **2006**, *128*, 8590–8606. (c) Geng, C.; Ye, S.; Neese, F. *Angew. Chem., Int. Ed.* **2010**, *49*, 5717–5720. (d) Wilson, S. A.; Chen, J.; Hong, S.; Lee, Y.-M.; Clémancey, M.; Garcia-Serres, R.; Nomura, T.; Ogura, T.; Latour, J.-M.; Hedman, B.; Hodgson, K. O.; Nam, W.; Solomon, E. I. *J. Am. Chem. Soc.* **2012**, *134*, 11791–11806.
- (10) (a) Decker, A.; Clay, M. D.; Solomon, E. I. *J. Inorg. Biochem.* **2006**, *100*, 697–706. (b) Neidig, M. L.; Decker, A.; Choroba, O. W.; Huang, F.; Kavana, M.; Moran, G. R.; Spencer, J. B.; Solomon, E. I. *Proc. Natl. Acad. Sci. U.S.A.* **2006**, *103*, 12966–12973. (c) Shaik, S.; Chen, H.; Janardanan, D. *Nat. Chem.* **2011**, *3*, 19–27. (d) Wong, S. D.; Bell, C. B., III; Liu, L. V.; Kwak, Y.; England, J.; Alp, E. E.; Zhao, J.; Que, L., Jr.; Solomon, E. I. *Angew. Chem., Int. Ed.* **2011**, *50*, 3215–3218. (e) Ye, S.; Neese, F. *Proc. Natl. Acad. Sci. U.S.A.* **2011**, *108*, 1228–1233. (f) Srnc, M.; Wong, S. D.; England, J.; Que, L., Jr.; Solomon, E. I. *Proc. Natl. Acad. Sci. U.S.A.* **2012**, *109*, 14326–14331.